

## RESEARCH ARTICLE

10.1002/2015JD023172

## Special Section:

Fast Physics in Climate Models: Parameterization, Evaluation and Observation

## Key Points:

- Momentum fluxes in high winds in shallow water were measured
- Impact of depth of water on the air-sea momentum flux
- Momentum fluxes were estimated by three methods and were compared

## Correspondence to:

Z. Gao,  
zgao@mail.iap.ac.cn

## Citation:

Bi, X., Z. Gao, Y. Liu, F. Liu, Q. Song, J. Huang, H. Huang, W. Mao, and C. Liu (2015), Observed drag coefficients in high winds in the near offshore of the South China Sea, *J. Geophys. Res. Atmos.*, 120, doi:10.1002/2015JD023172.

Received 28 JAN 2015

Accepted 10 JUN 2015

Accepted article online 19 JUN 2015

## Observed drag coefficients in high winds in the near offshore of the South China Sea

Xueyan Bi<sup>1,2,3</sup>, Zhiqiu Gao<sup>1</sup>, Yangang Liu<sup>3</sup>, Feng Liu<sup>4</sup>, Qingtao Song<sup>5,6</sup>, Jian Huang<sup>2</sup>, Huijun Huang<sup>2</sup>, Weikang Mao<sup>2</sup>, and Chunxia Liu<sup>2</sup>

<sup>1</sup>State Key Laboratory of Atmospheric Boundary Layer Physics and Atmospheric Chemistry, Institute of Atmospheric Physics, Chinese Academy of Sciences, Beijing, China, <sup>2</sup>Guangzhou Institute of Tropical and Marine Meteorology, China Meteorological Administration/Guangdong Provincial Key Laboratory of Regional Numerical Weather Prediction, Guangdong, China, <sup>3</sup>Brookhaven National Laboratory, Upton, New York, USA, <sup>4</sup>Climate and Atmospheric Science Section, Division of Illinois State Water Survey, Prairie Research Institute, University of Illinois at Urban-Champaign, Champaign, Illinois, USA, <sup>5</sup>National Satellite Ocean Application Service, Beijing, China, <sup>6</sup>Key Laboratory of Space Ocean Remote Sensing and Application, SOA, Beijing, China

**Abstract** This paper investigates the relationships between friction velocity, 10 m drag coefficient, and 10 m wind speed using data collected at two offshore observation towers (one over the sea and the other on an island) from seven typhoon episodes in the South China Sea from 2008 to 2014. The two towers were placed in areas with different water depths along a shore-normal line. The depth of water at the tower over the sea averages about 15 m, and the depth of water near the island is about 10 m. The observed maximum 10 min average wind speed at a height of 10 m is about  $32 \text{ m s}^{-1}$ . Momentum fluxes derived from three methods (eddy covariance, inertial dissipation, and flux profile) are compared. The momentum fluxes derived from the flux profile method are larger (smaller) over the sea (on the island) than those from the other two methods. The relationship between the 10 m drag coefficient and the 10 m wind speed is examined by use of the data obtained by the eddy covariance method. The drag coefficient first decreases with increasing 10 m wind speed when the wind speeds are  $5\text{--}10 \text{ m s}^{-1}$ , then increases and reaches a peak value of 0.002 around a wind speed of  $18 \text{ m s}^{-1}$ . The drag coefficient decreases with increasing 10 m wind speed when 10 m wind speeds are  $18\text{--}27 \text{ m s}^{-1}$ . A comparison of the measurements from the two towers shows that the 10 m drag coefficient from the tower in 10 m water depth is about 40% larger than that from the tower in 15 m water depth when the 10 m wind speed is less than  $10 \text{ m s}^{-1}$ . Above this, the difference in the 10 m drag coefficients of the two towers disappears.

## 1. Introduction

The dependence of the drag coefficient ( $C_D$ ) on wind speed under tropical cyclone conditions is critically important for understanding and modeling storm intensity [Rogers *et al.*, 2013; Soloviev *et al.*, 2014]. On the basis of a theoretical study of the energy balance of a typhoon system, Emanuel [1995] argued that storm intensity depends on the ratio of the enthalpy coefficient ( $C_k$ ) to  $C_D$  and the ratio lies in the range of 0.75–1.5 in the high wind region of intense storms. The  $C_k$  has little relation to wind speed [Jeong *et al.*, 2012], that means  $C_D$  does not continue to increase at higher wind speeds. The idea of sea surface drag saturation at high wind speed has attracted the attention of several research communities and has been confirmed by subsequent field observations [Powell *et al.*, 2003; Black *et al.*, 2007; French *et al.*, 2007; Jarosz *et al.*, 2007; Holthuijsen *et al.*, 2012], laboratory experiments [Alamaro *et al.*, 2002; Donelan *et al.*, 2004; Troitskaya *et al.*, 2012], modeling studies [Moon *et al.*, 2004; Bye and Jenkins, 2006; Zweers *et al.*, 2010], and theoretical studies [Emanuel, 2003; Makin, 2005]. These studies show that when the saturation 10 m drag coefficient ( $C_{D10}$ ) falls between 0.002 and 0.0025, the corresponding  $\bar{u}_{10}$  is approximately  $30\text{--}33 \text{ m s}^{-1}$  [Powell *et al.*, 2003; Donelan *et al.*, 2004; French *et al.*, 2007; Jarosz *et al.*, 2007; Holthuijsen *et al.*, 2012]. However, the relationship between  $C_{D10}$  and  $\bar{u}_{10}$  in strong storms has been examined mainly over deep water. Limited field experiments were conducted over shallow water under high wind speeds, and details of the relationship between  $C_{D10}$  and  $\bar{u}_{10}$  remain unresolved [Ancil and Donelan, 1996; Zachry *et al.*, 2013a; Liu *et al.*, 2012]. Drag coefficient parameterizations for deep water are commonly applied to shallow water. Additional and improved field measurements are essential to gaining a better understanding of  $C_D$  behavior under high wind conditions over shallow water.

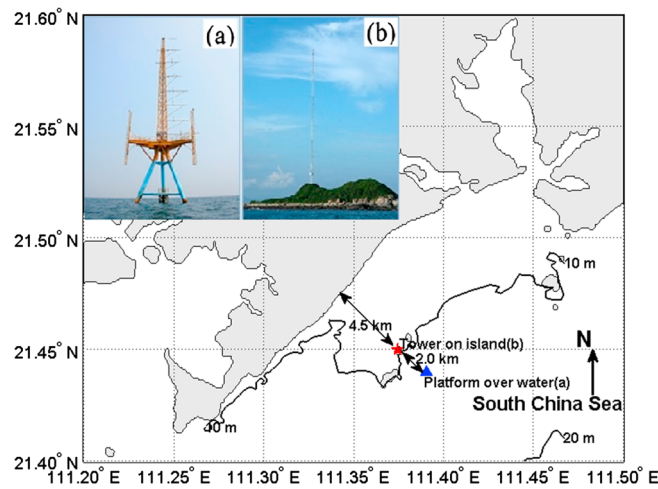


**Figure 1.** An illustration of the platforms and locations of the tower over water (blue upward pointing triangle) and the tower on Zhizai Island (red pentagram). The bathymetric contours (m) are also shown.

Seven typhoon cases (Hagupit, Chanthu, Nockten, Nesat, Kaitak, Rammasun, and Kalmaegi) were captured from 2008 to 2014 at two offshore instrumented towers (Figure 1). With observations from two buoys anchored 6.7 and 81.9 km from the towers, *Zhao et al.* [2015] estimated the relative water depth (0.9) near the towers during typhoons, which is much less than the threshold (3) for shallow-water conditions. The relative water depth is equal to  $n \times h$ , where  $n$  is the wave number and  $h$  is the water depth. The main objective of this paper is to examine the relationships between the friction velocity ( $u_*$ ),  $C_{D10}$ , and  $\bar{u}_{10}$  over shallow water under high wind conditions by using these unique observations.

## 2. Experimental Setup

The data were collected at two offshore towers fixed along the shore-normal line during seven typhoon events from 2008 to 2014. Figure 1 shows a map of the two towers and the bathymetric contours around the towers. One tower ( $21^\circ26'24''N$ ,  $111^\circ23'26''E$ ; hereafter sea tower) is on an integrated observation platform for marine meteorology over the sea at Bohe, Maoming. It is operated by the Institute of Tropical and Marine Meteorology, China Meteorology Administration [*Huang and Chan*, 2011]. It stands 6.5 km offshore in water depth of 15 m in the South China Sea. The observation platform is about 11 m above the mean sea level (msl). Its upper part is a 25 m high steel tower. Wind, temperature, and humidity sensors are mounted on 2 m booms on five different planes (13.4 m, 16.4 m, 20.0 m, 23.4 m, and 31.3 m above msl) with a sampling frequency of 1 min. The models of these sensors are RM Young/05106 and HMP45C. Gill Windmaster Pro ultrasonic anemometers are installed on 2 m booms at 27.3 m and 35.1 m above msl with a sampling frequency of 10 Hz. A schematic view of the instruments deployed on this tower can be found in *Zhao et al.* [2013]. The other tower (hereinafter island tower), operated by the Guangdong Climate Centre, is on the Zhizai Island ( $21^\circ27'3.12''N$ ,  $111^\circ22'28''E$ ), about 2.0 km from the sea tower. The island has an above-water area of approximately  $90\text{ m} \times 40\text{ m}$  and is covered by sand and sparse weeds. The tower is 10 m above msl [*Wang et al.*, 2013]. The NRG #40 wind sensors are mounted on 2.5 m booms on six different planes (10.0 m, 20.0 m, 40.0 m, 60.0 m, 80.0 m, and 100.0 m above msl) with a sampling frequency of 1 min. Gill Windmaster Pro ultrasonic anemometers with a sampling frequency of 10 Hz were placed on the 2.5 m booms at a height of 60 m during Typhoon Hagupit and at a height of 40 m during Typhoon Chanthu. The instruments were placed on the east side of the towers facing the seaward direction to minimize flow distortion. The small island Dazhuzhou lies southwest of the towers. The instruments and measurements used in this work are listed in Table 1.

## 3. Characteristics of the Typhoons

Figure 2 shows the typhoon tracks relative to the location of the towers. Strong Typhoon ( $41.5\text{--}50.9\text{ m s}^{-1}$ ) Hagupit moved over the towers on 24 September 2008. The other six typhoons passed by south of the towers. Measurements from the sonic anemometers were collected for five typhoons, and the time series of observed wind speed (WS), wind direction (WD),  $\bar{u}_{10}$ , and distance of the typhoon center to the towers are shown in Figure 3. The red color indicates the portion of observations left after data quality control (detailed below). It can be seen from Figure 3 that the observations from the sonic anemometers are fairly consistent with those from the wind sensors. Typhoon Hagupit was the most intense storm observed from the towers, although Typhoon Chanthu had the highest  $\bar{u}_{10}$  of  $32\text{ m s}^{-1}$  based on the quality-controlled data. Figure 3 illustrates that from 4:30 to 6:00 A.M. on 24 September 2008 during Hagupit, the observed



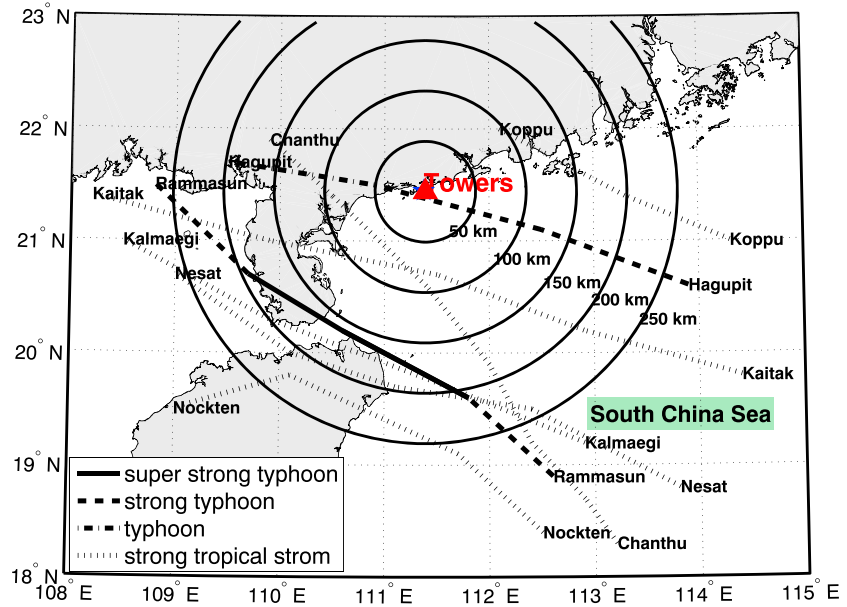


**Figure 2.** Map of the typhoon tracks along with the locations of the two observational towers. The different dashed lines denote the different typhoon categories. The black circles mark the distances to the towers of 50 km, 100 km, 150 km, 200 km, and 250 km. Super strong typhoon is larger than  $51 \text{ m s}^{-1}$ . Typhoon is from  $32.7 \text{ m s}^{-1}$  to  $41.4 \text{ m s}^{-1}$ , and strong tropical storm is from  $24.5 \text{ m s}^{-1}$  to  $32.6 \text{ m s}^{-1}$ . Note that the locations of the towers on the island (blue pentagon) and over the water (red upward pointing triangle) largely overlap each other due to their close proximity.

In this study we used three different methods to estimate  $u_*$ : eddy covariance, inertial dissipation, and flux profile methods. We also used the Coriolis correction of friction velocity given by *Donelan* [1990] in the analysis. To meet the neutral stability condition, the measurements with  $-0.1 < z/L < 0.1$  were chosen ( $L$  is the Obukhov length). For the measurements from the eddy covariance and the inertial dissipation methods,  $L$  is computed by

$$L = -\frac{u_*^3 \bar{T}_0}{gk w' \theta'_v}, \tag{4a}$$

where  $g$  is the gravitational acceleration,  $w' \theta'_v$  is the flux of virtual potential temperature at height  $z$ , and  $\bar{T}_0$  is the mean air temperature at height  $z$ . For the measurements using the flux profile method,  $L$  is estimated from the gradient Richardson number ( $Ri$ ) based on an empirical relationship proposed by *Arya* [1982]:

$$\frac{z}{L} = Ri \quad (Ri < 0)$$

$$\frac{z}{L} = \frac{Ri}{1 - 5 \cdot Ri} \quad (Ri > 0), \tag{4b}$$

where  $Ri$  is the average  $Ri_z$ . Every  $Ri_z$  is calculated from observations in which two levels by

$$Ri_z = g\bar{T} \cdot \left[ \frac{\Delta\bar{T}}{(z_1 z_2)^{3/2}} + \Gamma_d \right] \cdot \left( \frac{\ln \frac{z_2}{z_1}}{\Delta\bar{u}} \right)^2 \cdot z_1 z_2, \tag{5}$$

where  $z = \sqrt{z_1 z_2}$ ;  $\bar{T}$  is the mean temperature at height  $z$ ;  $\Delta\bar{T} = \bar{T}_2 - \bar{T}_1$ ,  $\Delta\bar{u} = \bar{u}_2 - \bar{u}_1$  and  $\bar{T}_1$  and  $\bar{T}_2$  are the temperatures at heights  $z_1$  and  $z_2$ , respectively; and  $\Gamma_d = 0.0098 \text{ K m}^{-1}$  is the dry adiabatic lapse rate.

#### 4.1. Eddy Covariance Method

In the eddy covariance method, friction velocity is directly calculated from the measurements of turbulent velocity fluctuations:

$$u_{*s} = \left( (\overline{u'w'})^2 + (\overline{v'w'})^2 \right)^{1/4}, \tag{6}$$

where  $u'$ ,  $v'$ , and  $w'$  are the turbulent fluctuations of the three wind components. The over bar indicates Reynolds averaging, and  $u_{*s}$  is the friction velocity without the Coriolis correction.

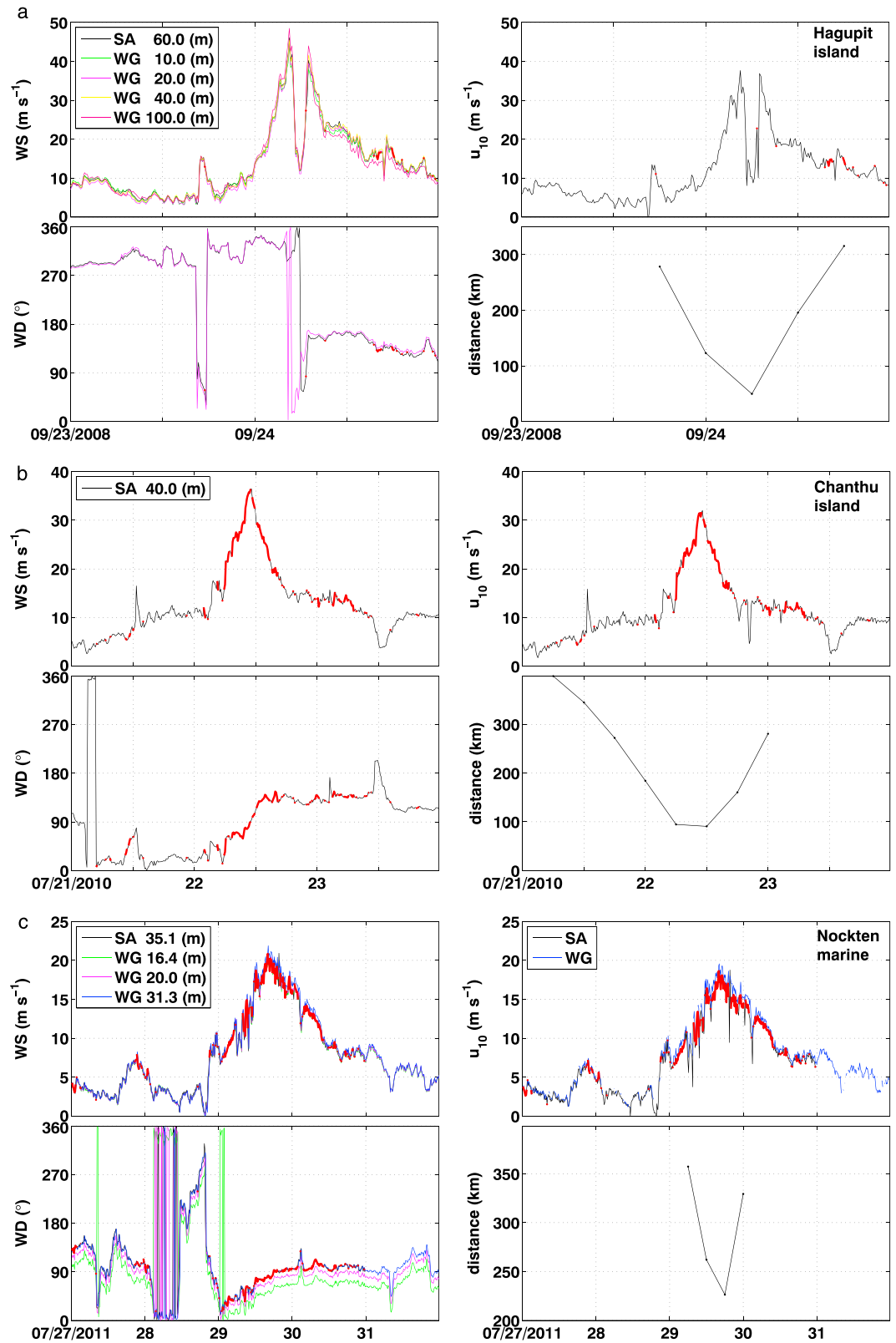


**Figure 3.** Temporal changes of the raw 10 min wind speed (WS), wind direction (WD) obtained from the sonic anemometers and the standard wind gauge, 10 m wind speed ( $u_{10}$ ) obtained by using a logarithmic wind profile (i.e., equation (3)), and the distance of the typhoon centers to the towers (data obtained from the website <http://www.typhoon.gov.cn/>). The red color represents the portion of observations from sonic anemometers left after quality control.

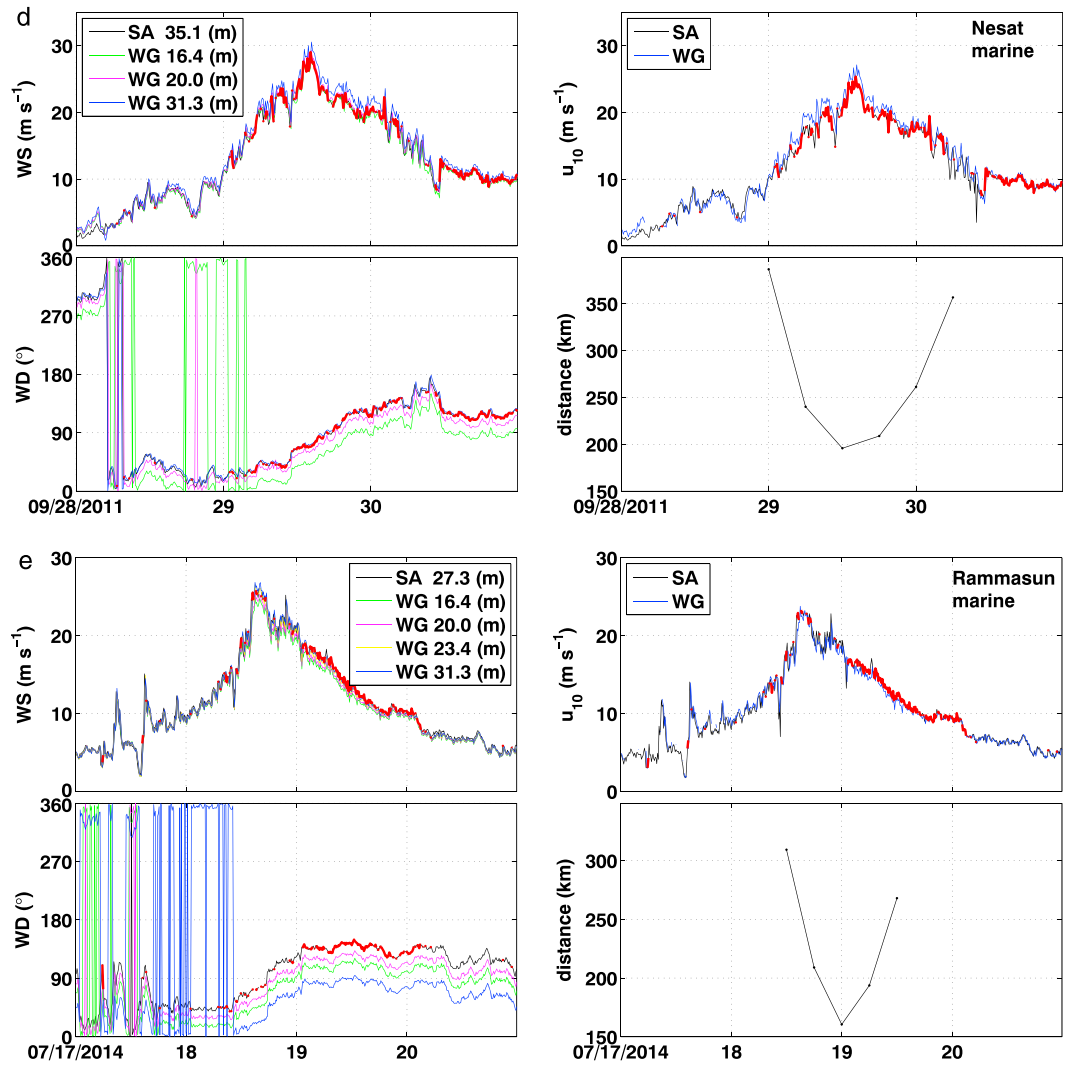


Figure 3. (continued)

**4.2. Inertial Dissipation Method**

Assuming that the dissipation of kinetic energy is balanced by the production of turbulence by the shear flow in the surface layer at the same level [Sjöblom and Smedman, 2004],  $u_{*s}$  is estimated by

$$u_{*s}^3 = kz\varepsilon/\varphi_\varepsilon, \tag{7}$$

where  $\varepsilon$  is the rate of dissipation of turbulent kinetic energy and  $\varphi_\varepsilon$  is the dimensionless dissipation function of stability and equals one under neutral conditions.

The dissipation rate  $\varepsilon$  is further related to the power spectral density  $S_u(f)$  of the streamline direction wind speed via [Panofsky and Dutton, 1984]

$$\varepsilon = \left[ f^{5/3} S_u(f) / (\alpha_u \bar{u}^{2/3}) \right]^{3/2}, \tag{8}$$

where the Kolmogorov's constant  $\alpha_u = 0.52$  and  $f$  is the frequency.

**4.3. Flux Profile Method**

The flux profile method is based on the logarithmic wind profile relationship:

$$u = \frac{u_{*s}}{k} \cdot \ln(z/z_0), \tag{9}$$

where  $z_0$  is the sea surface roughness length and  $u_{*s}/k$  is the slope of the least squares fitting of  $u$  and  $\ln(z)$ .

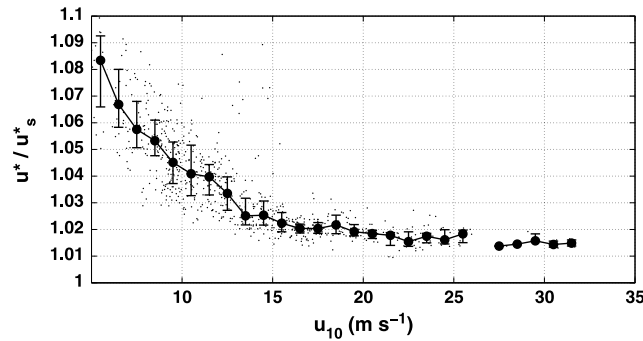


**Figure 4.** Ratio of the friction velocity obtained with the Coriolis correction ( $u_*$ ) to that without the Coriolis correction ( $u_{*s}$ ) as a function of 10 m wind speed ( $u_{10}$ ). The data are obtained from the eddy covariance method. The symbols and bars represent the median values and interquartile ranges, respectively.

Figure 4 shows that the ratio of  $u_*$  to  $u_{*s}$  decreases with increasing  $\bar{u}_{10}$ . For  $\bar{u}_{10} = 10\text{--}15\text{ m s}^{-1}$ ,  $u_{*s}$  underestimates  $u_*$  by approximately 3%–10%. For  $\bar{u}_{10} > 15\text{ m s}^{-1}$ ,  $u_{*s}$  underestimates  $u_*$  by about 2%.

#### 4.4. Coriolis Correction

Strictly speaking, a constant stress layer occurs only at the equator (no Coriolis acceleration) in stationary and homogeneous conditions; thus, the use of  $u_{*s}$  as the surface friction velocity  $u_*$  introduces a systematic underestimation of  $u_*$ . Donelan [1990] introduced equation (10) to correct this so-called Coriolis bias:

$$u_* = u_{*s}^2 \left( 1 + \frac{\alpha_0 f_c z}{u_{*s}} \right), \quad (10)$$

where  $\alpha_0 \approx 12$  for neutral conditions, and  $f_c = 1.454 \times 10^{-4} \sin(la)\text{ s}^{-1}$  is the Coriolis parameter, where  $la$  is the latitude. This Coriolis correction is applied in our analysis. We also examine it as a function of  $\bar{u}_{10}$ .

## 5. Data Processing and Quality Control

### 5.1. Sonic Anemometer Observations Preprocessing

Sonic anemometer measurements are crucial to both the eddy covariance method and the inertial dissipation method, as indicated in equations (6) and (7), respectively. It is necessary to apply several corrections to raw sonic anemometer data to produce fluctuations and means [Foken et al., 2005; Lee et al., 2005; Oh et al., 2010a]. Eddy covariance data processing has been widely investigated in previous studies [Lee et al., 2005] and consists of several steps: spike detection, coordinate rotation, and detrending to separate the turbulent signals from the mean flow [Lee et al., 2005]. Each step of the process can be approached in various ways, and selection of specific approaches depends upon both site and weather conditions [Vickers and Mahrt, 1997; Mauder et al., 2007, 2008]. In this work, the raw eddy covariance data were processed by the following steps:

#### 1. Spike detection and removal

Spike detection is similar to that of Hojstrup [1993]. A point is considered a spike and is discarded if it falls outside the prescribed limits. The prescribed limits are  $60\text{ m s}^{-1}$  for the horizontal wind speed,  $10\text{ m s}^{-1}$  for the vertical wind speed, and  $0\text{--}50^\circ\text{C}$  for air temperature. A point is also considered a spike if it is greater than 6 standard deviations of the difference between consecutive data points of a 10 min record. The data are not treated as spikes if four or more are detected consecutively. The discarded spikes are replaced by linearly interpolated values. A record is eliminated if the number of spikes is greater than 1% of the total number of data points in a 10 min segment.

#### 2. Averaging period

The choice of the averaging period is considered a crucial factor in turbulent flux calculation using the eddy covariance method. The Ogive method is used to determine an optimal averaging period at any site [Lee et al., 2005]:

$$Og_{uw}(f_0) = \int_{\infty}^{f_0} Co_{uw}(f) df, \quad (11)$$

where  $Co_{uw}(f)$  is the cospectrum of  $uw$  at frequency  $f$ . The Ogive curve shows the cumulative contribution of eddies of increasing period (decreasing frequency) to the total transport and reaches a constant after the frequency falls below a certain value. The time period corresponding to this frequency represents the minimum averaging time necessary to capture significant flux-carrying eddies. Figure 5 shows the Ogive of  $uw$  at different wind speeds during Typhoon Hagupit at a height of 60 m from the island tower. It is clear that the Ogive curve approaches a constant at an averaging period of 10 min, which we chose as the averaging period in our calculation of turbulent fluxes.

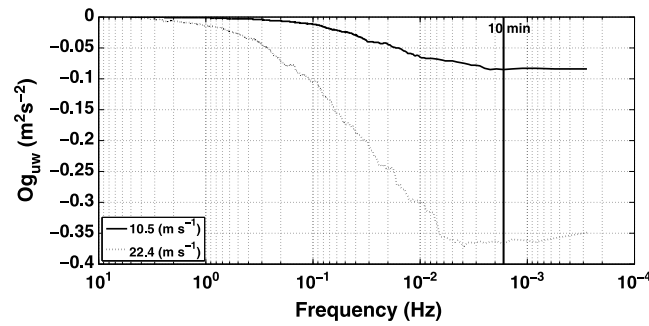


**Figure 5.** Ogives from the consecutive 30 min average spectrum of  $uw$  measured during Hagupit over the island at 60 m height (the solid line is for a wind speed of  $10.5 \text{ m s}^{-1}$ ; the dashed line is for a wind speed of  $22.4 \text{ m s}^{-1}$ ). The 10 min averaging time applied in this study is marked by the vertical line.

3. Coordinate rotation (tilt correction) and detrending

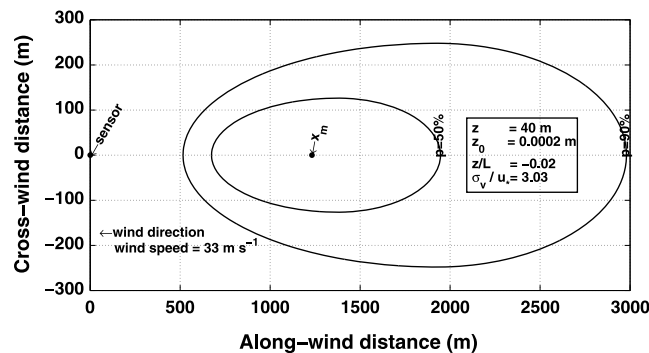
The coordinate system of the sonic measurements is transformed into the mean-flow streamlines to eliminate instrument tilt errors and cross contamination among components of the turbulent flux vector [Finnigan, 2004; Oh et al., 2010b]. We applied the double rotation approach [Kaimal and Finnigan, 1994] in this work (it is introduced in detail in the Appendix A). The detrending method uses a block time average recommended by Lee et al. [2005] to separate means and turbulent components. The dominant

wind direction at the towers is easterly. In order to minimize the influence of flow distortion by the platform, the data observed on the sea tower with wind directions between  $240^\circ$  and  $300^\circ$  are removed. Considering the influence of flow distortion by Dazhuzhou Island, we also removed the data observed on the tower on Zhizai Island with wind directions between  $180^\circ$  and  $300^\circ$ .

**5.2. Footprint Analysis**

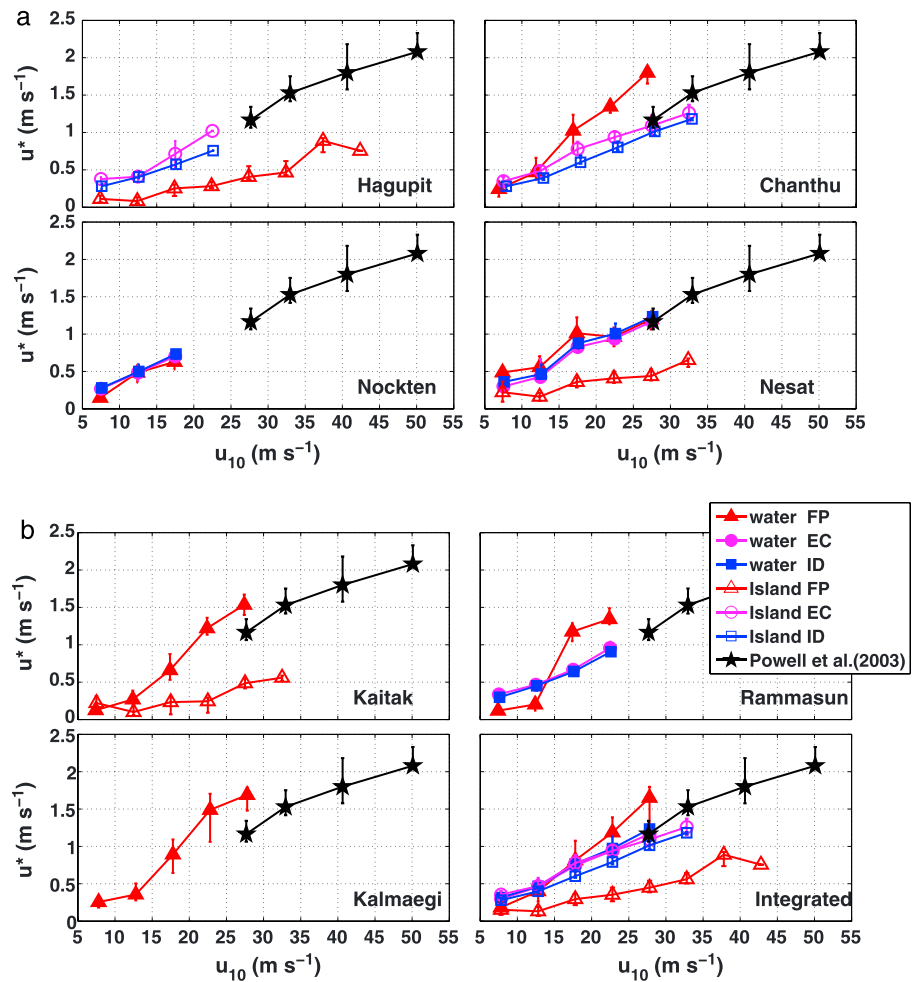
The footprint analysis method is usually applied to identify the region that influences the flux measurements. Schmid [1994] recommends the Eulerian analytic scalar flux source area model (FSAM) for those fluxes obtained from the eddy covariance method, and the Eulerian analytic scalar concentration source area model (SAM) for those obtained from the flux profile, the Bowen ratio, or other indirect methods, which rely on observations of mean concentrations. FSAM and SAM are both based on the inverted plume assumption and require the parameters— $\bar{u}$ ,  $z$ ,  $z_0$ , and  $z/L$ , and the intensity of crosswind turbulence ( $\frac{\sigma_w}{u_*}$ ) as inputs.

Figure 6 shows the 50% and 90% of the surface source areas of fluxes obtained from the eddy covariance method on the island for wind speeds of  $33.0 \text{ m s}^{-1}$  at a height of 40 m during Typhoon Chanthu. The symbol  $x_m$  represents the maximum source weight location. Figure 6 shows clearly that 90% of the source area upwind distances from the sensors are between 500 m and 3000 m when the wind speed is  $33 \text{ m s}^{-1}$  at a height of 40 m. As stated in section 2, Zhizai Island is 4.5 km from the shore and has an above water area of approximately  $90 \text{ m} \times 40 \text{ m}$ . It is clear that the minimum distance of the surface 90% source area from the sensors is about 500 m, larger than the 90 m of the Zhizai Island area. The maximum distance of the surface 90% source area from the sensors is about 3.0 km, less than the 4.5 km from the island to the shore. So the fluxes obtained by the eddy covariance method on the island should not be influenced by either the island or the shore.



**Figure 6.** The 50% and 90% flux source areas by the eddy covariance method on the island tower for winds of  $33.0 \text{ m s}^{-1}$  at a height of 40 m during Typhoon Chanthu. The symbol  $x_m$  indicates the maximum source location (upwind distance of the surface element with the maximum influence on the sensor).

Because there were no standard temperature sensors on the island tower, the  $z/L$  cannot be obtained from the flux profile method and the corresponding footprint cannot be analyzed. However, Schmid [1997] indicates that measurements obtained from the flux profile method are influenced by the local surface patch. That is to say, measurements obtained from the flux profile method on the island are influenced by the island. This may be a key reason for the differences between the fluxes obtained from the eddy covariance and the flux profile methods on the island (shown in section 6.1).



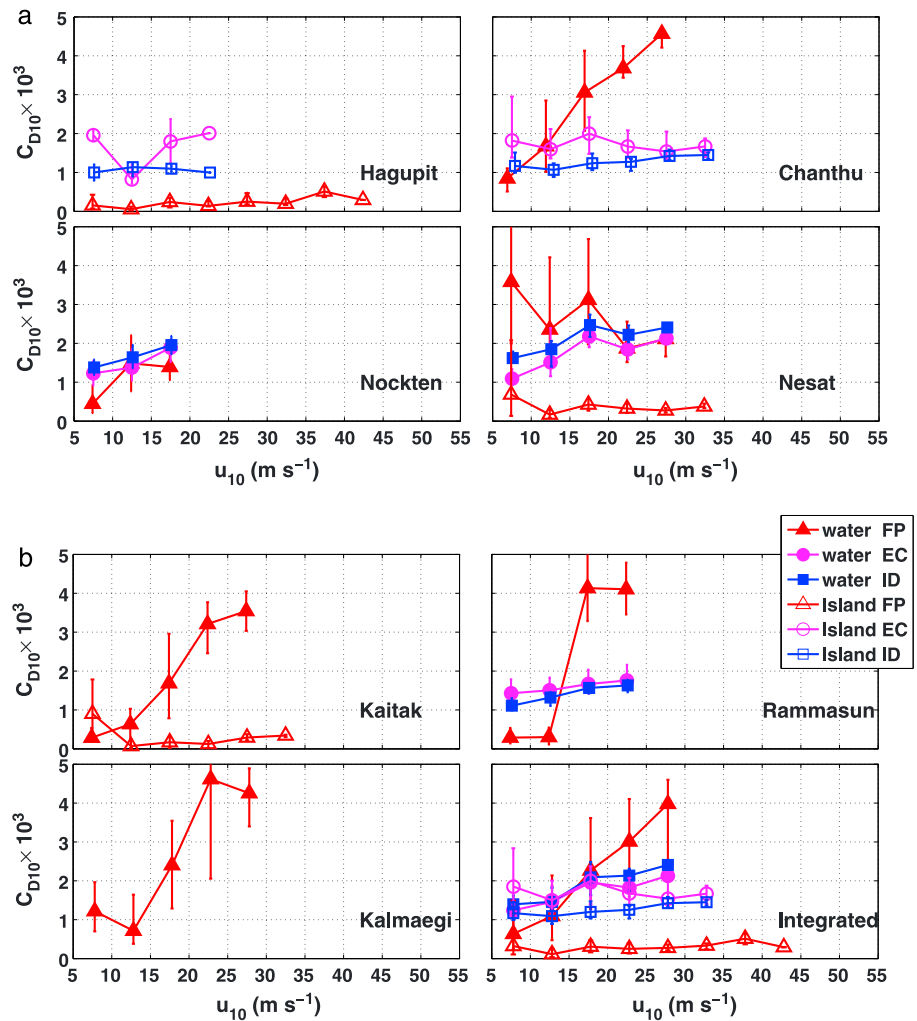
**Figure 7.** The values of the friction velocity ( $u_*$ ) derived from the eddy correlation method (EC) (magenta), the inertial dissipation method (ID) (blue), and the flux profile method (FP) (red) as a function of 10 m wind speed ( $u_{10}$ ) during different typhoon events. The solid (hollow) symbols denote the observations from the sea (island) tower. The symbols and bars represent the median values and interquartile ranges, respectively. The  $u_{10}$  bin size is  $5 \text{ m s}^{-1}$ . The results given by Powell et al. [2003] are also shown for comparison (black pentagon).

## 6. Results and Discussion

### 6.1. Comparison Between Different Methods

The momentum fluxes can be estimated using the eddy covariance method, the inertial dissipation method, or the flux profile method, each of which has advantages and disadvantages. The eddy covariance method, the direct method for calculating the fluxes using the high-frequency data, is sensitive to platform motion and sensor tilt and suffers from sampling uncertainty. The inertial dissipation and flux profile methods are insensitive to platform motion and distortion of airflow but rely on the validity of similarity theory. The eddy covariance and the inertial dissipation methods use some of the same data, but while the eddy covariance method directly estimates  $u_*$ , the inertial dissipation method equates production and dissipation turbulent kinetic energy and derives the latter from the spectrum of the streamwise velocity component. Over land in moderate wind conditions, the eddy covariance method is generally thought to be superior.

Figure 7 (Figure 8) compares the values of  $u_*$  ( $C_{D10}$ ) obtained by the three methods as a function of  $\bar{u}_{10}$  for each typhoon case and for all cases combined. It is evident that  $u_*$  and  $C_{D10}$  obtained from the eddy covariance and the inertial dissipation methods on both towers have similar patterns. However, the results derived from the flux profile method show that both  $u_*$  and  $C_{D10}$  are larger (smaller) on the sea (island) tower than those from the other two methods.



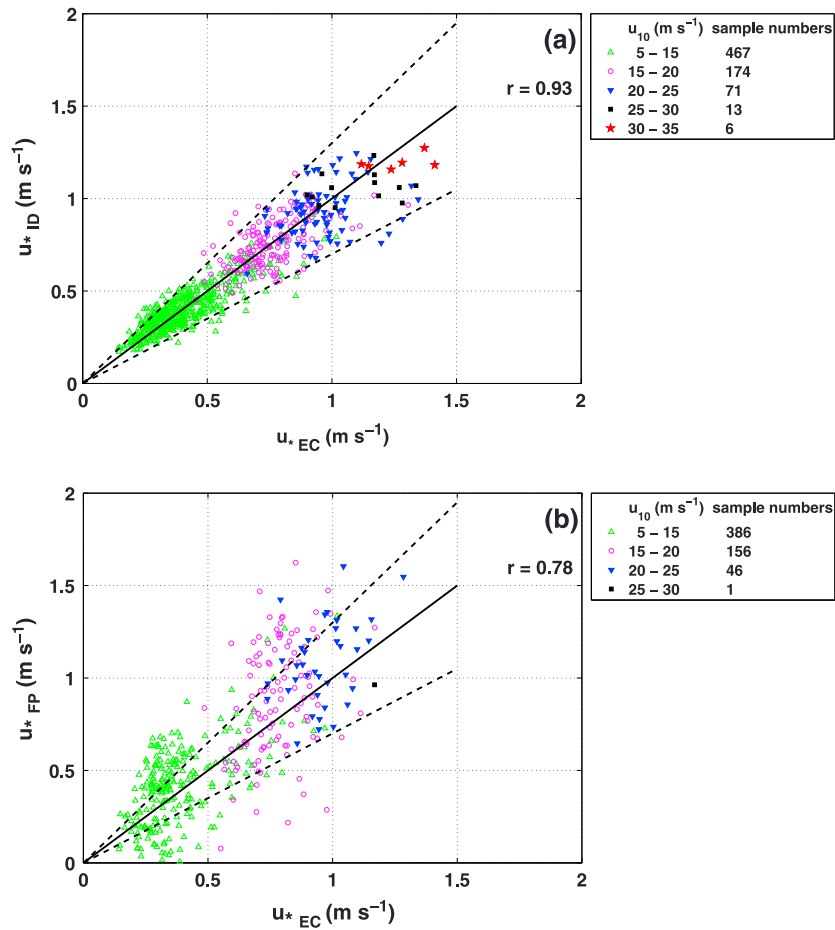
**Figure 8.** The same as Figure 7 except for the drag coefficient ( $C_{D10}$ ) as a function of 10 m wind speed ( $u_{10}$ ).

Figure 9a further compares the simultaneous  $u_*$  derived from the eddy covariance and inertial dissipation methods. The correlation coefficient is 0.93, and 88.1% of the data points concentrate between lines  $y = (1 + 30\%)x$  and  $y = (1 - 30\%)x$ . Figure 9b compares  $u_*$  from the eddy covariance and flux profile methods. The correlation coefficient is 0.78, and only 28.5% of the data points concentrate between lines  $y = (1 + 30\%)x$  and  $y = (1 - 30\%)x$ . It is clear that the inertial dissipation method better correlates with the eddy covariance method than with the flux profile method. Thus, only the measurements obtained from the eddy covariance method are analyzed in the remaining analysis.

The different results from the flux profile method compared to the other two methods can be attributed to (1) the island influences the fluxes obtained from the flux profile method on the island (as discussed in section 5.2), (2) the flux profile method used the data collected at two levels which are influenced by different fetches, and (3) the inherent errors in slow response anemometers significantly influence the accuracy of the flux profile method that uses the wind speed difference between two levels to calculate the flux. The flux profile method has been used for many years for turbulent flux calculation. It is valid for homogeneous surfaces such as open ocean surfaces [Powell et al., 2003].

**6.2. Impact of Height on Momentum Flux and Drag Coefficient**

Because there were no simultaneous measurements at different heights, we compared the median values of  $u_*$  and  $C_{D10}$  binned according to a  $5 \text{ m s}^{-1}$  of  $\bar{u}_{10}$  interval for each typhoon case. Figure 10 shows the values of



**Figure 9.** The friction velocity obtained using (a) the inertial dissipation method ( $u_{*ID}$ ) and (b) the flux profile method ( $u_{*FP}$ ) compared to those obtained by using the eddy correlation method ( $u_{*EC}$ ). The dashed lines indicate the  $\pm 30\%$  deviations from the solid 1:1 line, and  $r$  is a correlation coefficient. The different colors denote different ranges of 10 m wind speed ( $u_{10}$ ).

$u_*$  and  $C_{D10}$  as functions of  $\bar{u}_{10}$  for each typhoon case. The results indicate that neither relationship varies systematically with height. This suggests the validity of the constant stress layer hypothesis in this work.

### 6.3. Impact of Water Depth on the Air-Sea Momentum Flux

As shown in Figure 1, the two towers are placed in areas with different water depths along a shore-normal line. The water depth at the sea tower averages about 15 m [Huang and Chan, 2011], and the water depth near Zhizai Island is about 10 m. Donelan et al. [2012] showed that water depth ( $< 30$  m) has a strong effect on  $C_{D10}$  during strong winds. The observations at the towers provide an opportunity to investigate the impact of water depth on momentum flux in shallow water. Figure 10 shows the values of  $u_*$  and  $C_{D10}$  as functions of  $\bar{u}_{10}$  for each typhoon case. The magenta (blue) denotes the observations from the island (sea) tower. Below  $10 m s^{-1}$ ,  $C_{D10}$  is about 0.0018 on the island tower and is about 0.00125 on the sea tower. The values of  $C_{D10}$  in 10 m water depth are about 40% larger than those in 15 m. This difference of 40% is larger than measurement uncertainties, which were about 10–15% for neutral conditions [Kessomkiat et al., 2013]. Anctil and Donelan [1996] observed that the value of  $C_{D10}$  is about 0.0028 in 4 m water depth and about 0.0018 in 12 m depth when  $\bar{u}_{10}$  is  $14 m s^{-1}$ . Limited previous field campaigns and laboratory measurements found that  $C_{D10}$  is higher over shallow water than over deep water at wind speeds below hurricane force because of the markedly different wave conditions [Anctil and Donelan, 1996; Zachry et al., 2013a, 2013b]. Our measurements support this conclusion, but only when  $\bar{u}_{10} < 10 m s^{-1}$ . Beyond  $10 m s^{-1}$ , the difference in  $C_{D10}$  between the two towers disappears. Unfortunately, no simultaneous wave data were available near

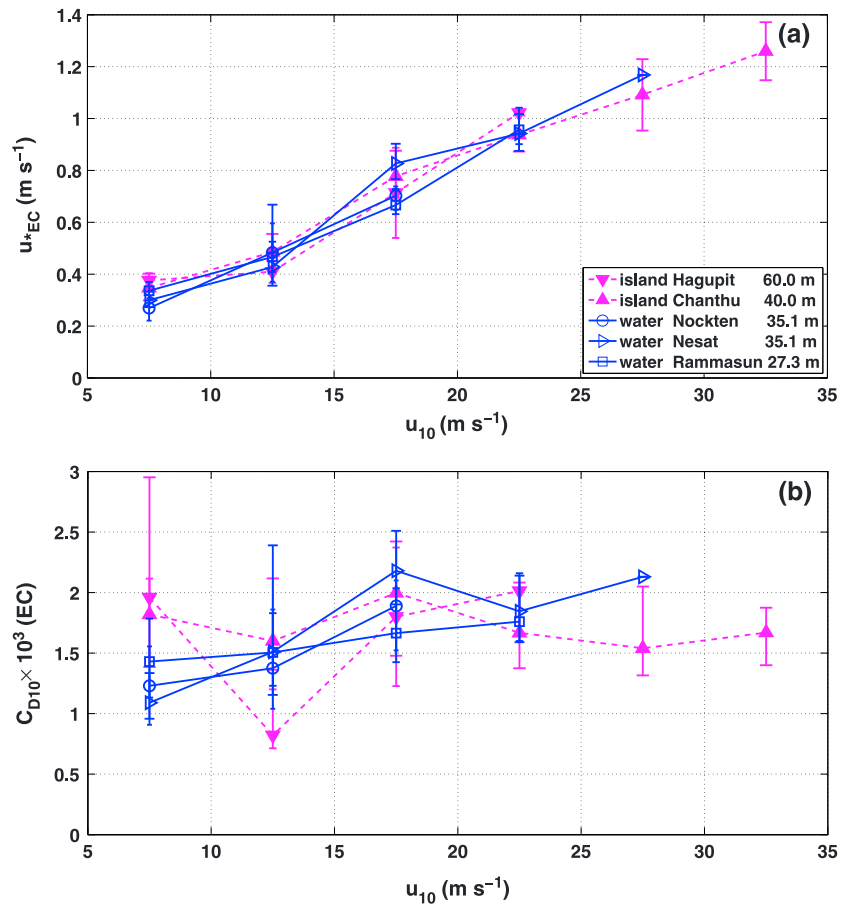


**Figure 10.** The values of (a) the friction velocity ( $u_{*EC}$ ) and (b) the 10 m neutral drag coefficient ( $C_{D10}$ ) derived from the eddy correlation (EC) method as a function of 10 m wind speed ( $u_{10}$ ) during different typhoon events. The symbols and bars represent the median values and interquartile ranges, respectively. The  $u_{10}$  bin size is  $5 \text{ m s}^{-1}$ . The solid magenta (blue) symbols denote the observations from the tower over the island (water).

the observation platform for further analysis. This reinforces the conclusion evident in Figure 6 that the fluxes obtained from the eddy covariance method on the island are solely influenced by the sea surface not by the island or shore. Therefore, we combine the observations from the two towers and perform a composite analysis.

**6.4. Characteristics of Friction Velocity and Drag Coefficient**

Figure 11 shows that the values of  $u_*$  and  $C_{D10}$  yielded from the eddy covariance method as a function of  $\bar{u}_{10}$ , with the data derived from the five typhoon events combined. The median values and interquartile ranges binned according to  $5 \text{ m s}^{-1}$  intervals of  $u_{10}$  are shown; also shown are the sample numbers in every bin. For the sake of clarity, the median values are also shown in  $1 \text{ m s}^{-1}$  bins. Figure 11a shows that  $u_*$  increases with increasing  $\bar{u}_{10}$  when  $\bar{u}_{10} = 5 - 35 \text{ m s}^{-1}$ . The values of  $u_*$  are less than those reported by Powell et al. [2003] for  $\bar{u}_{10} = 25 - 35 \text{ m s}^{-1}$ . Figure 11b shows that  $C_{D10}$  initially decreases with increasing  $\bar{u}_{10}$  for  $\bar{u}_{10} = 5 - 10 \text{ m s}^{-1}$ , then increases and reaches a peak at  $\bar{u}_{10} = 18 \text{ m s}^{-1}$  before decreasing again, and then levels off beyond  $27 \text{ m s}^{-1}$ . When  $\bar{u}_{10} = 10 - 18 \text{ m s}^{-1}$ ,  $C_{D10}$  increases with  $\bar{u}_{10}$  in much the same manner as reported in Large and Pond [1981]. However, below  $10 \text{ m s}^{-1}$  and above  $18 \text{ m s}^{-1}$ , our measurements show a quite different pattern from those previously reported [Powell et al., 2003; Donelan et al., 2004; Jarosz et al., 2007]. Our measurements are larger for  $\bar{u}_{10} = 5 - 10 \text{ m s}^{-1}$  but are smaller for  $\bar{u}_{10} > 18 \text{ m s}^{-1}$ . The values for the saturation  $C_{D10}$  of 0.002 are similar to those of Powell et al. [2003] and French et al. [2007], but the saturation  $\bar{u}_{10}$  of  $18 \text{ m s}^{-1}$  is much less than the  $30-35 \text{ m s}^{-1}$  reported by others.

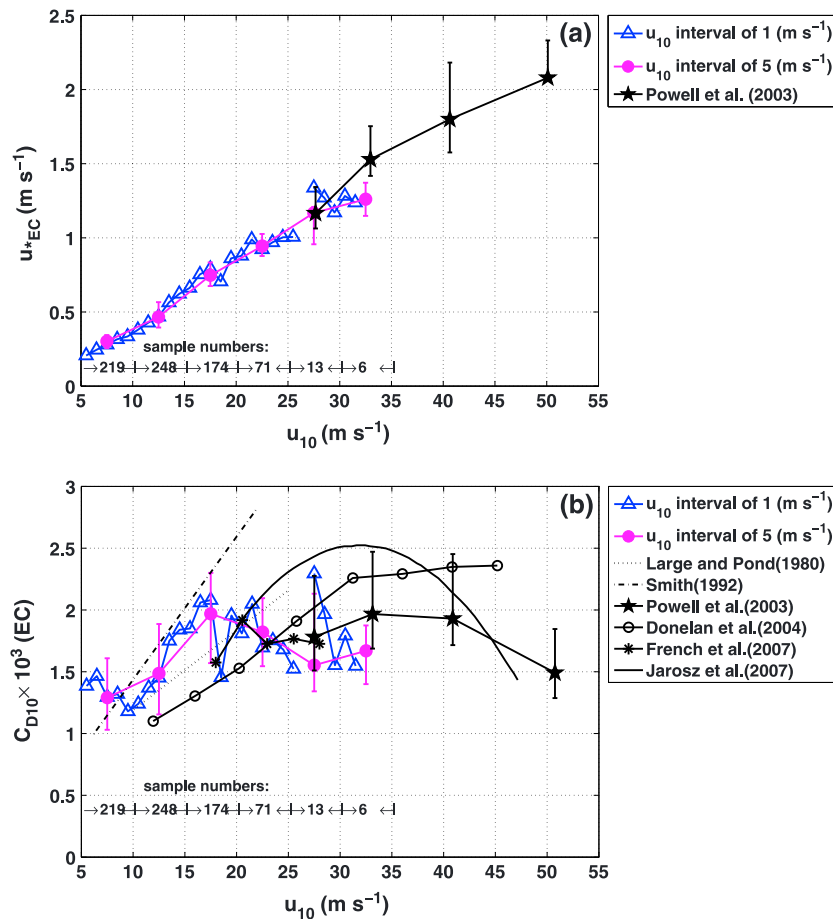


**Figure 11.** Relationships of (a) the friction velocity ( $u_{*EC}$ ) and (b) the 10 m drag coefficient ( $C_{D10}$ ) (derived from the eddy correlation method) as a function of 10 m wind speed ( $u_{10}$ ) for five integrated typhoon events. The blue upward pointing triangles and magenta solid circles represent the median values binned according to 1 m s<sup>-1</sup> and 5 m s<sup>-1</sup> of  $u_{10}$  interval, respectively. The corresponding bars represent the interquartile ranges. Also shown are the data points or fitting curves reported in literature for comparison.

The discrepancies may have arisen from numerous factors related to the conditions of the sea, such as water depth. Since depth-induced wave breaking becomes an important dissipation term in a sloping bed surf zone as at our research sites [Holthuijsen et al., 2012; Richter and Sullivan, 2013], a shoaling effect can lead to a lower saturation  $\bar{u}_{10}$ .

In order to better demonstrate the influence of wind-wave conditions on  $C_{D10}$ , Figure 12 also shows  $C_{D10}$  as a function of  $\bar{u}_{10}$  in different wind directions: 0–90° is the right front quadrant of a typhoon and 90–180° is the right rear quadrant. Observations from Coupled Boundary Layer and Air-Sea Transfer reveal the distinctively different wave spectra in the different storm quadrants in association with the sea state. However, the value of  $C_{D10}$  is independent of the storm quadrant [Black et al., 2007]. Our measurements also show that there are no obvious differences in  $C_{D10}$  between different quadrants of typhoons.

### 7. Conclusions

Measurements collected from two offshore towers in the South China Sea during seven typhoon cases are examined. Analysis of the measurements from the two towers, placed in regions of 10 m and 15 m water depths along a shore-normal line, supports the existing notion that  $C_{D10}$  is higher in shallower water when wind speeds are below hurricane force but only for  $\bar{u}_{10} < 10$  m s<sup>-1</sup>. Beyond 10 m s<sup>-1</sup>, the difference in  $C_{D10}$  between the two towers disappears. The dependence of  $C_{D10}$  on  $\bar{u}_{10}$  shows a different pattern when  $\bar{u}_{10} = 5 - 10$  m s<sup>-1</sup> and  $\bar{u}_{10} = 18 - 27$  m s<sup>-1</sup>:  $C_{D10}$  decreases with increasing  $\bar{u}_{10}$  and levels off beyond

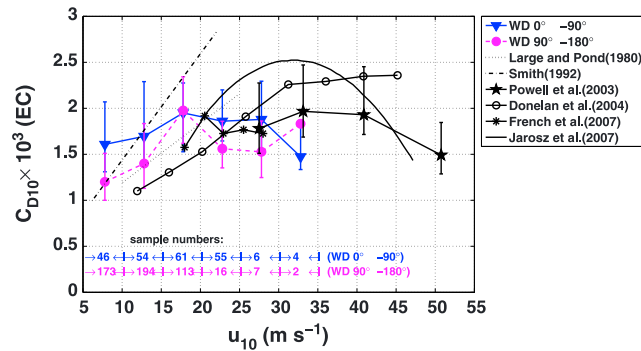


**Figure 12.** Relationship of the 10 m drag coefficient ( $C_{D10}$ ) (derived from the eddy correlation method) as a function of 10 m wind speed ( $u_{10}$ ) in different wind directions for five integrated typhoon events. The blue solid downward pointing triangles (magenta solid circles) and bars represent the median values and interquartile ranges in wind directions of 0–90° (90–180°). The  $u_{10}$  bin size is  $5 \text{ m s}^{-1}$ . Also shown for comparison are the data points or fitting curves reported in literature.

$27 \text{ m s}^{-1}$ . The value of saturation  $C_{D10}$  of 0.002 is similar to the results of Powell et al. [2003] and French et al. [2007], but saturation  $\bar{u}_{10} = 18 \text{ m s}^{-1}$  is significantly less than other observations of  $30\text{--}35 \text{ m s}^{-1}$ . The value of  $C_{D10}$  is independent of the typhoon quadrant. The interaction between waves and the local bathymetry that causes wave conditions to dramatically change in shallow water under high winds may be responsible for these results. Unfortunately, no simultaneous wave data were available near the towers for comparison with those in deep water.

Three commonly used methods for estimating the momentum fluxes (eddy covariance, inertial dissipation, and flux profile methods) are compared, and the comparison shows that the results obtained from the eddy covariance and the inertial dissipation methods are in good agreement. The relationships between  $u_*$ ,  $C_{D10}$ , and  $\bar{u}_{10}$  do not exhibit a systematic change with measurement height. This supports the existence of a constant stress layer. The results derived from the flux profile method on the sea (island) tower are larger (smaller) than that from the other two methods, suggesting that the island influenced the fluxes derived from the flux profile method and thus caution is needed in using the flux profile method over a heterogeneous surface.

Three commonly used methods for estimating the momentum fluxes (eddy covariance, inertial dissipation, and flux

profile methods) are compared, and the comparison shows that the results obtained from the eddy covariance and the inertial dissipation methods are in good agreement. The relationships between  $u_*$ ,  $C_{D10}$ , and  $\bar{u}_{10}$  do not exhibit a systematic change with measurement height. This supports the existence of a constant stress layer. The results derived from the flux profile method on the sea (island) tower are larger (smaller) than that from the other two methods, suggesting that the island influenced the fluxes derived from the flux profile method and thus caution is needed in using the flux profile method over a heterogeneous surface.

### Appendix A: Coordinate Rotation (Double Rotation)

Double rotation is based on works by Tanner and Thurtell [1969], as proposed by Aubinet et al. [2000]. It is related to period-by-period rotation, which can be accomplished for every data averaging period (10 min). Two rotations are conducted. The first rotation is around the z axis into the mean wind such that  $\bar{v}_1 = 0$ :

$$\begin{aligned} u_1 &= u_m \cos \theta + v_m \sin \theta \\ v_1 &= -u_m \sin \theta + v_m \cos \theta, \\ w_1 &= w_m \end{aligned}$$

where  $u_m$ ,  $v_m$ , and  $w_m$  are the observed wind speeds in three coordinate axes and  $\theta = \tan^{-1}(\bar{v}_m/\bar{u}_m)$ . The symbols  $\bar{u}_m$  and  $\bar{v}_m$  are the mean wind speeds along the x and y axes;  $u_1$ ,  $v_1$ , and  $w_1$  are the wind speeds in the new coordinate system after the first rotation; and  $\bar{u}_1$ ,  $\bar{v}_1$ , and  $\bar{w}_1$  are the mean values of  $u_1$ ,  $v_1$ , and  $w_1$ .

The second rotation is around the new y axis, so that  $\bar{w}_2 = 0$ :

$$\begin{aligned} u_2 &= u_1 \cos \phi + w_1 \sin \phi \\ v_2 &= v_1 \\ w_2 &= -u_1 \sin \phi + w_1 \cos \phi \end{aligned}$$

where  $\phi = \tan^{-1}(\bar{w}_1/\bar{u}_1)$ . The symbols  $u_2$ ,  $v_2$ , and  $w_2$  are the wind speeds in the new coordinate system after these two rotations. Having performed these rotations, the coordinate system of the sonic anemometer is moved into alignment with the mean streamlines.

### Acknowledgments

This work was supported by the National Natural Science Foundation of China under grants 40906023, 41205011, 41475061, 41175013, 41076012, and 41276019 and the National Program on Key Basic Research Project of China (973) under grant 2011CB403501. This work is also supported by the U.S. DOE ESM via the FASTER project (<http://www.bnl.gov/esm/>) and ASR program. The authors are particularly grateful to D. Richter and two anonymous reviewers for their careful reviews and valuable comments, which led to substantial improvement of this manuscript. We thank all the crew members who took part in the campaigns and collected the valuable data. The authors would like to also thank Zhiqun Shi and Wenchao Chen of the Guangdong Climate Centre for their help with the data on the tower on Zhizai Island. We thank our colleague, Zhongkuo Zhao for a lot of useful discussion and help in data processing. The data and code (in MATLAB formats) used in this paper can be obtained from the first author.

### References

- Alamaro, M., K. Emanuel, J. Colton, W. McGillis, and J. Edson (2002), Experimental investigation of air-sea transfer of momentum and enthalpy at high wind speed paper presented at Preprints, 25th Conf. on Hurricanes and Tropical Meteorology, Am. Meteorol. Soc., San Diego, Calif.
- Ancil, F., and M. A. Donelan (1996), Air-water momentum flux observations over Shoaling waves, *J. Phys. Oceanogr.*, *26*(7), 1344–1353, doi:10.1175/1520-0485(1996)026<1344:amfoos>2.0.co;2.
- Arya, S. P. (1982), Atmospheric boundary layers over homogeneous terrain, in *Engineering Meteorology*, edited by E. J. Plate, pp. 233–267, Elsevier, New York.
- Aubinet, M., J. Moncrieff, R. C. Clement, M. Aubinet, J. Moncrieff, and R. C. Clement (2000), Estimates of the annual net carbon and water exchange of forests: The EUROFLUX methodology, *Adv. Ecol. Res.*, *30*, 113–175.
- Black, P. G., E. A. D'Asaro, T. B. Sanford, W. M. Drennan, J. A. Zhang, J. R. French, P. P. Niiler, E. J. Terrill, and E. J. Walsh (2007), Air–sea exchange in hurricanes: Synthesis of observations from the Coupled Boundary Layer Air–Sea Transfer Experiment, *Bull. Am. Meteorol. Soc.*, *88*(3), 357–374, doi:10.1175/bams-88-3-357.
- Bye, J. A. T., and A. D. Jenkins (2006), Drag coefficient reduction at very high wind speeds, *J. Geophys. Res.*, *111*, C03024, doi:10.1029/2005JC003114.
- Donelan, M. A. (1990), Air–sea interaction. The Sea, in *Ocean Engineering Science*, vol. 9, edited by B. LeMéhauté and D. M. Hanes, 250 pp., John Wiley, New York.
- Donelan, M. A., B. K. Haus, N. Reul, W. J. Plant, M. Stiassnie, H. C. Graber, O. B. Brown, and E. S. Saltzman (2004), On the limiting aerodynamic roughness of the ocean in very strong winds, *Geophys. Res. Lett.*, *31*, L18306, doi:10.1029/2004GL019460.
- Donelan, M. A., M. Curcic, S. S. Chen, and A. K. Magnusson (2012), Modeling waves and wind stress, *J. Geophys. Res.*, *117*, C00J23, doi:10.1029/2011JC007787.
- Dyer, A. J. (1974), A review of flux-profile relationships, *Boundary-Layer Meteorol.*, *7*(3), 363–372, doi:10.1007/BF00240838.
- Emanuel, K. A. (1995), Sensitivity of tropical cyclones to surface exchange coefficients and a revised steady-state model incorporating eye dynamics, *J. Atmos. Sci.*, *52*(22), 3969–3976, doi:10.1175/1520-0469(1995)052<3969:sotcts>2.0.co;2.
- Emanuel, K. A. (2003), A similarity hypothesis for air–sea exchange at extreme wind speeds, *J. Atmos. Sci.*, *60*(11), 1420–1428, doi:10.1175/1520-0469(2003)060<1420:ashfae>2.0.co;2.
- Finnigan, J. J. (2004), A re-evaluation of long-term flux measurement techniques Part II: Coordinate systems, *Boundary-Layer Meteorol.*, *113*(1), 1–41, doi:10.1023/b:boun.0000037348.64252.45.
- Foken, T., M. Göckede, M. Mauder, L. Mahrt, B. Amiro, and W. Munger (2005), *Handbook of Micrometeorology: Post-Field Data Quality Control*, edited by X. Lee, W. Massman, and B. Law, pp. 181–208, Springer, Netherlands, doi:10.1007/1-4020-2265-4\_9.
- French, J. R., W. M. Drennan, J. A. Zhang, and P. G. Black (2007), Turbulent fluxes in the hurricane boundary layer. Part I: Momentum flux, *J. Atmos. Sci.*, *64*(4), 1089–1102, doi:10.1175/jas3887.1.
- Garratt, J. R. (1992), *The Atmospheric Boundary Layer*, pp. 41–55, Cambridge Univ. Press, Cambridge.
- Hojstrup, J. (1993), A statistical data screening procedure, *Meas. Sci. Technol.*, *4*(2), 153.
- Holthuijsen, L. H., M. D. Powell, and J. D. Pietrzak (2012), Wind and waves in extreme hurricanes, *J. Geophys. Res.*, *117*, C09003, doi:10.1029/2012JC007983.
- Huang, J., and P.-W. Chan (2011), Progress of marine meteorological observation experiment at Maoming of south China, *J. Trop. Meteorol.*, *17*(4), 418–429, doi:10.3969/j.issn.1006-8775.2011.04.012.
- Jarosz, E., D. A. Mitchell, D. W. Wang, and W. J. Teague (2007), Bottom-up determination of air-sea momentum exchange under a major tropical cyclone, *Science*, *315*(5819), 1707–1709, doi:10.1126/science.1136466.
- Jeong, D., B. K. Haus, and M. A. Donelan (2012), Enthalpy transfer across the air–water interface in high winds including spray, *J. Atmos. Sci.*, *69*, 2733–2748, doi:10.1175/JAS-D-11-0260.1.
- Kaimal, J. C., and J. J. Finnigan (1994), *Atmospheric Boundary Layer Flows: Their Structure and Measurement*, 289 pp., Oxford Univ. Press, New York.
- Kessomkiat, W., H.-J. H. Franssen, A. Graf, and H. Vereecken (2013), Estimating random errors of eddy covariance data: An extended two-tower approach, *Agric. For. Meteorol.*, *171*–*172*(0), 203–219, doi:10.1016/j.agrformet.2012.11.019.
- Large, W. G., and S. Pond (1981), Open ocean momentum flux measurements in moderate to strong winds, *J. Phys. Oceanogr.*, *11*(3), 324–336, doi:10.1175/1520-0485(1981)011<0324:oomfmi>2.0.co;2.
- Lee, X., B. Law, and W. Massman (2005), *Handbook of Micrometeorology: A Guide for Surface Flux Measurement and Analysis*, Springer Science + Business Media, Inc., Dordrecht.
- Liu, C., Q. Wan, F. Liao, and Z. Zhao (2012), Surface observations in the tropical cyclone environment over the South China Sea, *J. Trop. Meteorol.*, *18*(2), 263–274, doi:10.3969/j.issn.1006-8775.2012.02.015.
- Liu, G., Y. Liu, and S. Endo (2013), Evaluation of surface flux parameterizations with long-term ARM observations, *Mon. Weather Rev.*, *141*(2), 773–797, doi:10.1175/mwr-d-12-00095.1.
- Makin, V. K. (2005), A note on the drag of the sea surface at hurricane winds, *Boundary-Layer Meteorol.*, *115*(1), 169–176, doi:10.1007/s10546-004-3647-x.
- Mauder, M., S. Oncley, R. Vogt, T. Weidinger, L. Ribeiro, C. Bernhofer, T. Foken, W. Kohsiek, H. R. Bruin, and H. Liu (2007), The energy balance experiment EBEX-2000. Part II: Intercomparison of eddy-covariance sensors and post-field data processing methods, *Boundary-Layer Meteorol.*, *123*(1), 29–54, doi:10.1007/s10546-006-9139-4.
- Mauder, M., T. Foken, R. Clement, J. Elbers, W. Eugster, T. Grünwald, B. Heusinkveld, and O. Kolle (2008), Quality control of CarboEurope flux data? Part 2: Inter-comparison of eddy-covariance software, *Biogeosciences*, *5*(2), 451–462.
- Moon, I.-J., I. Ginis, and T. Hara (2004), Effect of surface waves on air–sea momentum exchange. Part II: Behavior of drag coefficient under tropical cyclones, *J. Atmos. Sci.*, *61*(19), 2334–2348, doi:10.1175/1520-0469(2004)061<2334:eoswoa>2.0.co;2.
- Oh, H.-M., K.-J. Ha, K.-Y. Heo, K.-E. Kim, S.-J. Park, J.-S. Shim, and L. Mahrt (2010a), On drag coefficient parameterization with post processed direct fluxes measurements over the ocean, *Asia-Pac. J. Atmos. Sci.*, *46*(4), 513–523, doi:10.1007/s13143-010-0030-3.
- Oh, H.-M., K.-E. Kim, K.-J. Ha, L. Mahrt, and J.-S. Shim (2010b), Quality control and tilt correction effects on the turbulent fluxes observed at an ocean platform, *J. Appl. Meteorol. Climatol.*, *50*(3), 700–712, doi:10.1175/2010jamc2367.1.
- Panofsky, H. A., and J. A. Dutton (1984), *Atmospheric Turbulence: Models and Methods for Engineering Applications*, Wiley, New York.
- Powell, M. D., P. J. Vickery, and T. A. Reinhold (2003), Reduced drag coefficient for high wind speeds in tropical cyclones, *Nature*, *422*(6929), 279–283.
- Richter, D. H., and D. P. Stern (2014), Evidence of spray-mediated air-sea enthalpy flux within tropical cyclones, *Geophys. Res. Lett.*, *41*, 2997–3003, doi:10.1002/2014GL059746.
- Richter, D. H., and P. P. Sullivan (2013), Momentum transfer in a turbulent, particle-laden Couette flow, *Phys. Fluids* (1994-present), *25*(5), doi:10.1063/1.4804391.

- Rogers, R., et al. (2013), NOAA'S hurricane intensity forecasting experiment: A progress report, *Bull. Am. Meteorol. Soc.*, *94*(6), 859–882, doi:10.1175/BAMS-D-12-00089.1.
- Schmid, H. P. (1994), Source areas for scalars and scalar fluxes, *Boundary-Layer Meteorol.*, *67*(3), 293–318, doi:10.1007/bf00713146.
- Schmid, H. P. (1997), Experimental design for flux measurements: Matching scales of observations and fluxes, *Agric. Forest Meteorol.*, *87*(2–3), 179–200, doi:10.1016/S0168-1923(97)00011-7.
- Sjöblom, A., and A.-S. Smedman (2004), Comparison between eddy-correlation and inertial dissipation methods in the marine atmospheric surface layer, *Boundary-Layer Meteorol.*, *110*(2), 141–164, doi:10.1023/A:1026006402060.
- Smith, R. K., and M. T. Montgomery (2014), On the existence of the logarithmic surface layer in the inner core of hurricanes, *Q. J. R. Meteorol. Soc.*, *140*(678), 72–81, doi:10.1002/qj.2121.
- Soloviev, A. V., R. Lukas, M. A. Donelan, B. K. Haus, and I. Ginis (2014), The air-sea interface and surface stress under tropical cyclones, *Sci. Rep.*, *4*, doi:10.1038/srep05306.
- Tanner, C. B., and G. W. Thurtell (1969), Anemoclinometer measurements of Reynolds stress and heat transport in the atmospheric surface layer. ECOM 66-G22-F, ECOM United States Army Electronics Command, Research and Development.
- Troitskaya, Y. I., D. A. Sergeev, A. A. Kandaurov, G. A. Baidakov, M. A. Vdovin, and V. I. Kazakov (2012), Laboratory and theoretical modeling of air-sea momentum transfer under severe wind conditions, *J. Geophys. Res.*, *117*, C00J21, doi:10.1029/2011JC007778.
- Vickers, D., and L. Mahrt (1997), Quality control and flux sampling problems for tower and aircraft data, *J. Atmos. Oceanic Technol.*, *14*(3), 512–526, doi:10.1175/1520-0426(1997)014<0512:qcafsp>2.0.co;2.
- Wang, B., L. Song, and W. Chen (2013), Drag coefficient during strong typhoons, *Adv. Meteorol.*, *8*, doi:10.1155/2013/650971.
- Zachry, B. C., C. W. Letchford, D. Zuo, and A. B. Kennedy (2013a), Laboratory measurements of the drag coefficient over a fixed shoaling hurricane wave train, *Wind Struct. Int. J.*, *16*(2), 193–211, doi:10.12989/was.2013.16.2.193.
- Zachry, B. C., J. L. Schroeder, A. B. Kennedy, J. J. Westerink, C. W. Letchford, and M. E. Hope (2013b), A case study of nearshore drag coefficient behavior during hurricane Ike (2008), *J. Appl. Meteorol. Climatol.*, *52*(9), 2139–2146, doi:10.1175/jamc-d-12-0321.1.
- Zhao, Z., Z. Gao, D. Li, X. Bi, C. Liu, and F. Liao (2013), Scalar flux–gradient relationships under unstable conditions over water in coastal regions, *Boundary-Layer Meteorol.*, *148*(3), 495–516, doi:10.1007/s10546-013-9829-7.
- Zhao, Z.-K., C.-X. Liu, Q. Li, G.-F. Dai, Q.-T. Song, and W.-H. Lv (2015), Typhoon air-sea drag coefficient in coastal regions, *J. Geophys. Res. Oceans*, *120*, 716–727, doi:10.1002/2014JC010283.
- Zweers, N. C., V. K. Makin, J. W. de Vries, and G. Burgers (2010), A sea drag relation for hurricane wind speeds, *Geophys. Res. Lett.*, *37*, L21811, doi:10.1029/2010GL045002.